Accepted Author Manuscript

© 2026 IEEE. Personal use of this material is permitted. Permission from IEEE must be obtained for all other uses, in any current or future media, including reprinting/republishing this material for advertising or promotional purposes, creating new collective works, for resale or redistribution to servers or lists, or reuse of any copyrighted component of this work in other works.

A Computer Vision Approach to Automated Monitoring of Aeroponic Nozzle Operation

Sergey A. Galichenko
Department of Automation and Control
Moscow Polytechnic University
Moscow, Russia
sergeygalichenko.04@gmail.com

Evgeniy V. Pikalov
Department of Automation and Control
Moscow Polytechnic University
Moscow, Russia
e.v.pikalov@mail.ru

Abstract— Reliable aeroponic irrigation requires monitoring not only hydraulic parameters but also the spray formed inside the root chamber. This study experimentally evaluates a lightweight computer vision approach for monitoring aeroponic nozzle operation from conventional smartphone video. A laboratory installation with five nozzles was investigated under a reference five-nozzle condition and a controlled reduced condition in which the same two nozzles were closed. The evaluated descriptors included background difference, reference-relative binary coverage, Sobel, Canny, Laplacian of Gaussian responses, and Laplacian-variance sharpness. The main data set contained 26,319 frames from 44 irrigation cycles. Cycle-level analysis showed statistically significant separation between the three- and five-nozzle conditions for all evaluated descriptors, with the largest observed effect size for binary coverage. A separate benchmark on a Raspberry Pi 4 showed that each processing branch was individually compatible with a target rate of 30 frames per second. The results demonstrate the potential of image-based monitoring as a complementary diagnostic channel while also identifying limitations related to reference calibration, fixed optical conditions, and the non-randomized experimental sequence.

Keywords—aeroponics, computer vision, nozzle monitoring, spray analysis, background subtraction, image processing

I. Introduction

Aeroponics is a soilless cultivation technology in which plant roots are suspended in a root chamber and periodically supplied with nutrient solution through atomizing nozzles. Such systems provide direct control of root-zone conditions and can achieve high resource-use efficiency [1], [2]. Their operation, however, is strongly dependent on stable irrigation because the root zone lacks a moisture-retaining substrate. Consequently, nozzle configuration, pressure, irrigation timing, and monitoring are central design considerations [3]–[6]. Recent aeroponic monitoring systems commonly combine environmental and hydraulic sensing with automated pump control [4], [5], [7].

Pressure and flow measurements are important for monitoring the hydraulic circuit, but they do not completely describe the spatial result of nozzle operation. In a multi-nozzle system, the complete loss or partial degradation of an individual nozzle may change the visible extent and structure of the spray while causing a comparatively small change in total pressure or flow. A complementary diagnostic channel that directly observes spray formation can therefore provide information unavailable from integral hydraulic measurements. This distinction is especially important for fault scenarios that remain hydraulically subtle at system level. A nozzle can be completely or partially restricted while the common supply line still exhibits pressure and flow values within an acceptable range, particularly when several parallel nozzles are supplied simultaneously. The diagnostic problem addressed here is therefore not replacement of conventional instrumentation, but observation of the spatial manifestation of the irrigation process itself.

Image-based spray characterization has been investigated in agricultural and industrial applications. Acoustic nozzle monitoring has demonstrated the general feasibility of detecting pressure changes, clogging, and damage [8]. Optical approaches have been used to estimate spray angle and spatial distribution [9], segment agricultural spray patterns [10], monitor spray drift using infrared thermal imaging and image analysis [11], and compare image-derived spray distributions with volumetric measurements [12]. Machine vision has also been applied to irregular industrial nozzle patterns [13] and to fuel-spray morphology [14]–[16]. Earlier and recent studies further show that droplet and spray characteristics can be extracted from digital images using conventional image processing and statistical analysis [17]–[19].

These studies establish the diagnostic value of spray images, but many approaches target field sprayers, dedicated optical benches, or high-speed fuel-injection experiments. Aeroponic monitoring has a different objective: rather than resolving individual droplets or jet breakup, it must determine whether the observed spray is consistent with a reference operating state using compact hardware and computationally inexpensive processing. Experimental evaluation of such lightweight methods directly inside an aeroponic root chamber remains limited. For a compact aeroponic controller, however, the computational and optical complexity of the measurement system is an engineering constraint in its own right. A method based on a conventional camera and interpretable descriptors is attractive because it can be recalibrated to a particular chamber geometry, executed on general-purpose embedded hardware, and inspected by an operator without requiring a large labeled data set. This motivates the comparison of classical image-processing descriptors before introducing more complex learning-based models.

The aim of this study is to improve the diagnostic capability of automated aeroponic irrigation monitoring through image-based characterization of nozzle operation relative to a reference state. Background difference, reference-relative binary

Published version

S. Galichenko and E. Pikalov, “A Computer Vision Approach to Automated Monitoring of Aeroponic Nozzle Operation,” in 2026 International Ural Conference on Electrical Power Engineering (UralCon), Magnitogorsk, Russian Federation, IEEE, 2026, pp. 637–642.
doi: 10.1109/UralCon71028.2026.11734852 View on IEEE Xplore

coverage, edge-based descriptors, and image sharpness are evaluated under controlled pump-off, three-nozzle, and five-nozzle conditions. The study focuses on cycle-level separability of the operating conditions and on the computational feasibility of the evaluated methods for embedded implementation.

II. Experimental Setup and Methodology

A. Experimental Setup

Experiments were conducted on a laboratory-scale aeroponic installation with five nozzles mounted in a circular arrangement beneath the upper lid of the root chamber. A transparent window at the center of the lid provided an optical path for top-view recording. For every reduced-nozzle cycle, the same two nozzles were manually closed, leaving three active nozzles. The five-nozzle condition was treated as the reference operating state, while the three-nozzle condition represented a controlled partial-loss scenario rather than a complete model of real nozzle failure. The nozzles were located above the observed root-zone volume and directed into the chamber. Closing the same two nozzles preserved the mechanical geometry, illumination, and camera viewpoint while producing a repeatable reduction in the number of active spray sources. The resulting three-nozzle condition should therefore be interpreted as one reproducible reduced-operation configuration, not as a representation of every possible two-nozzle failure combination.

The experimental installation is shown in Fig. 1. The five nozzles were arranged circumferentially beneath the upper lid, with a transparent observation window located near the center of the lid. Experimental video sequences were recorded using a smartphone camera fixed above this window and directed vertically into the root chamber. The recordings used a resolution of 1920 × 1080 pixels at 30 frames/s. Camera position, field of view, installation geometry, and perimeter illumination were kept unchanged within each experimental series. Raspberry Pi 4 Model B was evaluated separately as the target embedded platform for computational benchmarking [20]; it was not used for acquisition of the experimental video data.

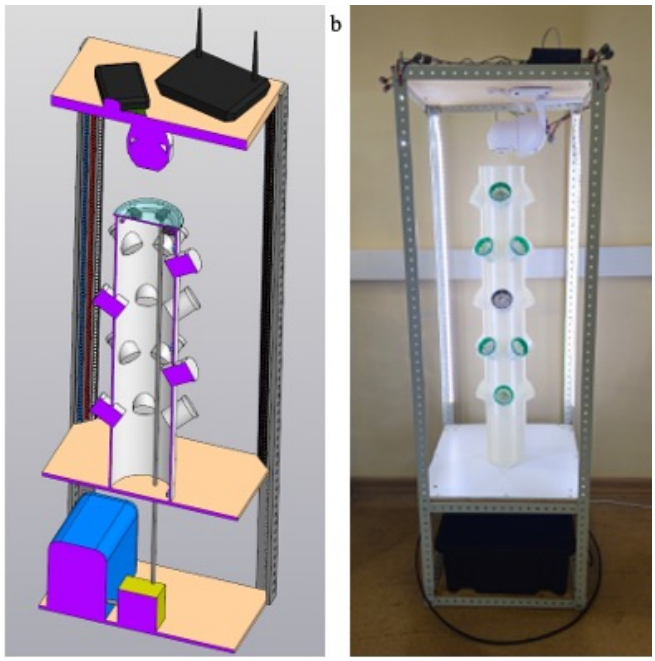


Fig. 1. Laboratory aeroponic installation used for the experiments: (a) CAD model; (b) laboratory prototype. During recording, the smartphone camera was positioned above the central transparent window in the upper lid (not shown).

B. Image Acquisition and Preprocessing

Two video data sets were analyzed. The transition series contained 2,585 frames and followed the sequence pump off–3 nozzles–off–5 nozzles–off–3 nozzles–off–5 nozzles–off, with 150 frames in each active interval. The main series contained 26,319 frames from 44 irrigation cycles. Cycles 1–22 corresponded to the five-nozzle condition and cycles 23–44 to the three-nozzle condition. A nominal complete cycle contained 600 frames. In the five-nozzle block, the 300-frame pump-on interval corresponded to frames 22–321 of each cycle; in the three-nozzle block it corresponded to frames 40–339. Although cycle 44 was incomplete overall, its complete pump-on interval was available and was retained for the active-state comparison.

Recorded color frames were converted to grayscale and processed using a fixed Gaussian smoothing stage before feature extraction. For difference-based processing, a median background was constructed from pump-off frames acquired under the same viewing geometry. Median estimation reduced the influence of isolated droplets, reflections, and frame-level noise. The preprocessing configuration was kept unchanged across the three- and five-nozzle experimental blocks so that no method was retuned for a particular operating condition.

C. Computer Vision Methods

The processing pipeline was implemented in C++ using OpenCV and was designed to characterize observable changes in the spray region rather than to resolve individual droplets. For a preprocessed frame $I_t(x, y)$ and the median pump-off background $B(x, y)$, the absolute background-difference map was defined as

$$D_t(x, y) = |I_t(x, y) - B(x, y)|. \quad (1)$$

The overall magnitude of the optical deviation from the background was represented by the normalized mean background difference

$$E_t = \frac{100}{255N} \sum_{(x,y)\in\Omega} D_t\,(x,y), \tag{2}$$

where Ω is the analyzed image region and $N = |\,\Omega\,|$ is the number of pixels within this region. Accordingly, E_t is expressed as a percentage of the 8-bit intensity range.

To estimate the spatial extent of sufficiently pronounced changes, the difference image was converted to a binary mask

$$M_t(x,y) = \begin{cases} 1, & D_t(x,y) \geq \tau^*, \\ 0, & D_t(x,y) < \tau^*, \end{cases} \tag{3}$$

and the corresponding binary coverage was calculated as

$$C_t = \frac{100}{N} \sum_{(x,y)\in\Omega} M_t\,(x,y). \tag{4}$$

Thus, C_t represents the percentage of the monitored image area whose difference from the background exceeds the calibrated threshold. It should not be interpreted as a direct measurement of wetted area or liquid deposition.

The segmentation threshold was determined automatically. Pump-off data were first used to establish the lower noise level, after which a histogram of difference values was accumulated during a reference pump-on calibration cycle. The operating threshold was selected according to

$$\tau^* = \max\{\tau \in \mathcal{T}: \bar{C}_{\mathrm{ref}}\,(\tau) \geq 85\%\}, \tag{5}$$

where $\mathcal{T}$ is the set of admissible thresholds and $\bar{C}_{\mathrm{ref}}\,(\tau)$ is the mean coverage obtained for the reference five-nozzle calibration data at threshold τ. Once selected, τ^* was held fixed during subsequent evaluation. Consequently, binary coverage is explicitly reference-relative, which must be considered when interpreting its statistical separation.

Three structural descriptors were additionally evaluated using Sobel, Canny, and Laplacian of Gaussian (LoG) processing. Their frame-level responses were based on the relative amount of detected structure in the corresponding binary response maps. These descriptors test whether changes in image structure provide diagnostic information complementary to direct background differencing. Spray can obscure stable scene boundaries while simultaneously creating local structures through droplets, streaks, and reflections.

Image sharpness was estimated using the variance of the Laplacian

$$S_t = \mathrm{Var}(\nabla^2 I_t)\,. \tag{6}$$

Sharpness was treated as an auxiliary scalar descriptor because its value can be affected not only by spray but also by focus, individual droplets, reflections, and contamination of the optical path.

In the recorded data, the raw Sobel, Canny, LoG, and sharpness responses decreased with increasing spray expression. For directional presentation, these descriptors were reflected using the affine transformation

$$\tilde{f}_t = f_{\max} + f_{\min} - f_t, \tag{7}$$

where $f_{\min}$ and $f_{\max}$ are the minimum and maximum observed values of the corresponding descriptor. This transformation reverses the direction and changes the offset of the scale but does not alter the within-group standard deviation, the magnitude of Cohen's d, or the significance obtained with Welch's t-test. Direction-aligned structural descriptors are therefore treated as arbitrary-unit diagnostic variables rather than as physical percentages.

Representative processing results for the reference five-nozzle and reduced three-nozzle conditions are shown in Figs. 2 and 3, respectively. The reduction in the number of active nozzles is most clearly visible in the background-difference images and in the spatial extent of the thresholded difference regions.

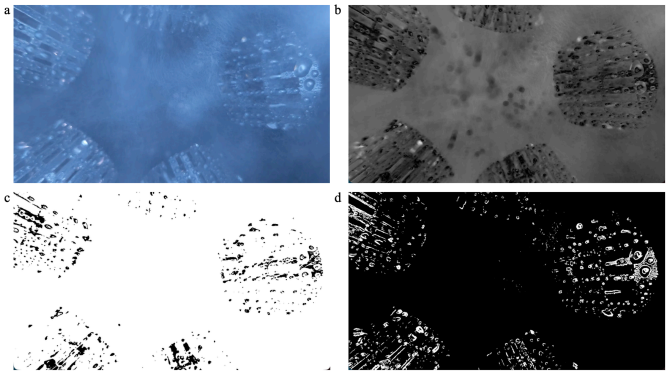


Fig. 2. Representative image-processing results for the reference five-nozzle condition: (a) original frame; (b) absolute background-difference image; (c) thresholded background-difference mask; (d) Sobel response.

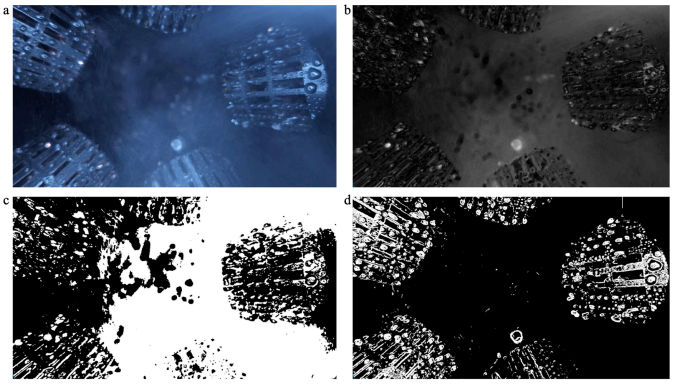


Fig. 3. Representative image-processing results for the reduced three-nozzle condition: (a) original frame; (b) absolute background-difference image; (c) thresholded background-difference mask; (d) Sobel response.

D. Experimental Procedure and Evaluation

Frame-level descriptors were aggregated at the irrigation-cycle level because consecutive video frames within one pump-on interval are strongly temporally correlated and cannot be treated as independent statistical observations. For each

descriptor f, the cycle-level value was calculated over the complete pump-on interval as

$$\bar{f}_c = \frac{1}{N_c}\sum_{t=1}^{N_c} f_{c,t}\,,\; N_c = 300, \tag{8}$$

where c denotes the irrigation cycle and N_c is the number of frames in the analyzed pump-on interval. For uniformly sampled video, this cycle mean is equivalent to the duration-normalized area under the descriptor curve and is used here because it has a more direct interpretation.

Pump-off intervals were used descriptively to characterize the no-spray baseline. Inferential statistical analysis was restricted to the two active operating conditions. The five-nozzle group contained 22 complete pump-on intervals and the three-nozzle group also contained 22 complete pump-on intervals. The latter includes cycle 44 because its pump-on segment was fully recorded despite the cycle being incomplete overall.

Differences between the active operating conditions were evaluated using Welch's two-sample t-test, which does not require equality of group variances. Separation magnitude was quantified using the absolute value of Cohen's d. A significance level of $p < 0.001$ is reported for the resulting comparisons.

Computational performance was evaluated separately using 425 recorded Full HD frames processed on a Raspberry Pi 4 Model B. Only OpenCV processing time was measured; camera acquisition, storage, network communication, and graphical visualization were excluded.

III. Results and Discussion

A. Response of Image Features to Nozzle Operation

The transition series showed clear and rapid changes in the image descriptors following changes in irrigation state. Background difference and binary coverage increased when spray was present and decreased after pump deactivation. The background-difference response decayed more slowly because residual spray remained visible in the chamber after liquid delivery stopped. Structural descriptors also changed consistently with the operating state, although their raw response direction was opposite to that of the difference-based descriptors. Short-lived deviations around switching events are consistent with residual pressure, individual droplets, and transient optical changes. These observations support cycle-level aggregation rather than diagnostic decisions based on individual frames.

For visualization of the transition series, the selected frame-level descriptors were additionally normalized relative to the maximum value obtained for the corresponding descriptor in the five-nozzle reference data:

$$R_f(t) = \frac{g_f(t)}{g_{f,\mathrm{ref}}^{\max}}, \tag{9}$$

where $g_f(t)$ denotes the descriptor after direction alignment, when applicable, and $g_{f,\mathrm{ref}}^{\max}$ is its maximum value in the reference five-nozzle data. Thus, $R_f = 1$ corresponds to 100% of the selected reference maximum. This normalization was used only for visualization of the temporal response and was not used in the cycle-level statistical analysis.

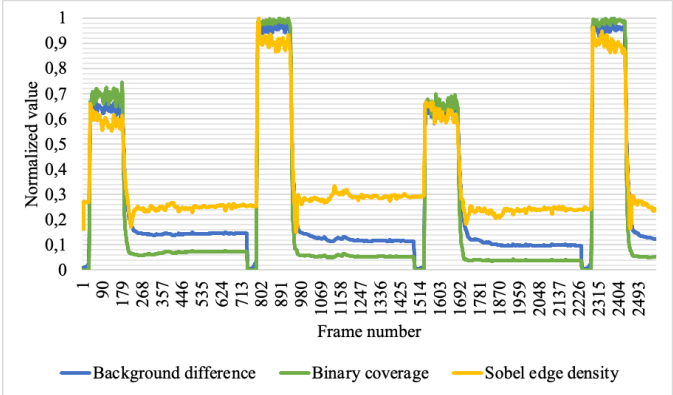


Fig. 4. Reference-normalized temporal responses of the background-difference, binary-coverage, and Sobel descriptors during the alternating pump-off–3-nozzle–pump-off–5-nozzle–pump-off–3-nozzle–pump-off–5-nozzle–pump-off sequence. A normalized value of 1 corresponds to the maximum value of the corresponding descriptor in the five-nozzle reference data.

All three descriptors responded consistently to changes in the irrigation state. The difference-based descriptors provided a clear separation between the three- and five-nozzle intervals, while the residual response observed after pump deactivation reflected the gradual dissipation of spray within the chamber.

Cycle-level values showed the same ordering for the two primary descriptors. Mean background difference increased from 3.68% of the 8-bit intensity range in pump-off intervals to 13.98 ± 0.60% for three active nozzles and 26.24 ± 0.76% for five active nozzles. Binary coverage increased from 5.37% of the frame in pump-off intervals to 31.93 ± 2.50% and 85.56 ± 1.56% for the three- and five-nozzle conditions, respectively. The value near 85% in the reference condition is consistent with the automatic calibration criterion and should therefore not be interpreted as an independent estimate of physical spray coverage.

B. Comparison of Image Processing Methods

All six evaluated descriptors showed statistically significant differences between the three- and five-nozzle pump-on conditions (Welch's two-sample t-test, $p < 0.001$). The cycle-level distributions exhibited low within-condition variability under the fixed experimental geometry, resulting in large standardized effect sizes. The largest separation was observed for binary coverage, followed by the direction-aligned Sobel descriptor and background difference. However, binary coverage is explicitly calibrated relative to the reference five-nozzle condition; its large effect size therefore indicates high sensitivity to deviations from that reference and should not be interpreted as evidence of universal superiority over the other descriptors. The cycle-level distributions of the evaluated descriptors are shown in Fig. 5. The limited overlap between the three- and five-nozzle groups is consistent with the low within-condition variability and the resulting large standardized effect

sizes. The corresponding numerical results are summarized in Table I.

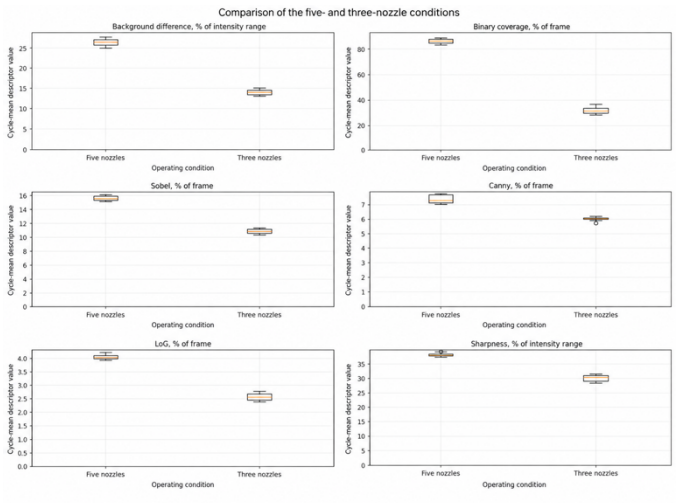


Fig. 5. Cycle-level distributions of the evaluated image descriptors for the reference five-nozzle and reduced three-nozzle conditions (n = 22 cycles per condition): (a) background difference; (b) binary coverage; (c) direction-aligned Sobel descriptor; (d) direction-aligned Canny descriptor; (e) direction-aligned Laplacian-of-Gaussian descriptor; (f) direction-aligned sharpness descriptor.

TABLE I. STATISTICAL COMPARISON OF THE THREE- AND FIVE-NOZZLE CONDITIONS.

Descriptor	Five nozzles, mean ± SD	Three nozzles, mean ± SD	$\lvert d \rvert$
Background difference, % intensity range	26.238 ± 0.760	13.981 ± 0.601	17.886
Binary coverage, % frame	85.562 ± 1.562	31.927 ± 2.504	25.704
Direction-aligned Sobel descriptor, a.u.	15.545 ± 0.256	10.838 ± 0.262	18.156
Direction-aligned Canny descriptor, a.u.	7.350 ± 0.265	6.036 ± 0.082	6.696
Direction-aligned LoG descriptor, a.u.	4.057 ± 0.080	2.577 ± 0.124	14.183
Direction-aligned sharpness descriptor, a.u.	38.118 ± 0.456	30.121 ± 0.876	11.450

Considering statistical separation, interpretability, and computational cost, background difference was selected as the primary descriptor. Unlike binary coverage, it does not depend on the reference-relative segmentation threshold and directly characterizes the magnitude of optical deviation from the current no-spray background. Binary coverage complements this information by describing the spatial extent of threshold-exceeding changes, while Sobel provides an additional structural descriptor. The remaining methods also separated the investigated conditions but offered less favorable combinations of interpretability, sensitivity, and robustness to local optical structure.

C. *Practical Applicability and Limitations*

The Raspberry Pi benchmark showed mean processing times of 13.34 ms for the combined background-difference and thresholding branch, 23.92 ms for Sobel, 27.71 ms for Canny, 17.26 ms for LoG, and 25.11 ms for sharpness. Each branch was therefore individually compatible with a 30 frames/s processing target at the algorithmic level. This result does not represent end-to-end throughput because acquisition, logging, communication, and visualization were excluded. The benchmark used recorded FHD frames and therefore evaluates computational cost of the algorithms rather than the complete camera-to-decision path. A production implementation should additionally measure acquisition latency, buffering, communication, and simultaneous execution of the selected descriptor set. The timing results nevertheless show that none of the individual processing branches alone requires specialized accelerator hardware for the tested image size.

Several limitations should be considered. First, the main series was recorded in consecutive blocks: all five-nozzle cycles preceded all three-nozzle cycles. Slow changes in condensation, illumination, or the optical scene therefore cannot be completely separated from the nozzle-state factor, although the transition series independently showed rapid descriptor changes when operating conditions were alternated. Second, the same two nozzles were closed in every reduced-nozzle cycle; different failed-nozzle locations may produce different spatial patterns. Third, the experiment modeled complete shutoff of two nozzles rather than partial clogging or progressive degradation. Finally, the segmentation threshold was calibrated relative to a reference operating cycle, so independent calibration data and validation under varying camera, illumination, and contamination conditions are required before deployment.

The vision descriptors characterize the visible spray within the camera field of view and do not directly measure nutrient-solution deposition on individual roots. Accordingly, the approach should be considered a complementary diagnostic channel rather than a replacement for pressure, flow, or other hydraulic measurements.

IV. CONCLUSION

This study experimentally evaluated a lightweight computer vision approach for monitoring aeroponic nozzle operation. Cycle-level analysis of 44 irrigation cycles showed strong separation between a reference five-nozzle condition and a controlled three-nozzle condition for all six investigated descriptors. Background difference provided the most direct and computationally inexpensive measure of optical deviation from the no-spray scene. Reference-relative binary coverage provided complementary information on the spatial extent of detected changes, while Sobel added structural information. All three- versus five-nozzle comparisons were statistically significant at $p < 0.001$.

A separate Raspberry Pi 4 benchmark showed that each processing branch was individually compatible with a 30 frames/s target at the algorithmic level. The results therefore support computer vision as an additional diagnostic source for compact aeroponic monitoring systems. Further validation should include randomized nozzle configurations, independent calibration data, partial clogging and gradual degradation scenarios, varying optical conditions, and methods for localization of individual nozzle faults.

REFERENCES

[1] I. A. Lakhiar, J. Gao, T. N. Syed, F. A. Chandio, and N. A. Buttar, "Modern plant cultivation technologies in agriculture under controlled

environment: a review on aeroponics," Journal of Plant Interactions, vol. 13, no. 1, pp. 338–352, 2018, doi: 10.1080/17429145.2018.1472308.

[2] A. Regmi, D. Rueda-Kunz, H. Liu, J. Trevino, S. Kathi, and C. Simpson, "Comparing resource use efficiencies in hydroponic and aeroponic production systems," Technology in Horticulture, vol. 4, no. 1, Art. no. e005, 2024, doi: 10.48130/tihort-0024-0002.

[3] I. A. Lakhiar, J. Gao, T. N. Syed, F. A. Chandio, N. A. Buttar, and W. A. Qureshi, "Monitoring and control systems in agriculture using intelligent sensor techniques: A review of the aeroponic system," Journal of Sensors, vol. 2018, Art. no. 8672769, 2018, doi: 10.1155/2018/8672769.

[4] A. P. Montoya, F. A. Obando, J. G. Morales, and G. Vargas, "Automatic aeroponic irrigation system based on Arduino's platform," Journal of Physics: Conference Series, vol. 850, Art. no. 012003, 2017, doi: 10.1088/1742-6596/850/1/012003.

[5] H. A. Méndez-Guzmán, J. A. Padilla-Medina, C. Martínez-Nolasco, J. J. Martinez-Nolasco, A. I. Barranco-Gutiérrez, L. M. Contreras-Medina, and M. Leon-Rodriguez, "IoT-based monitoring system applied to aeroponics greenhouse," Sensors, vol. 22, no. 15, Art. no. 5646, 2022, doi: 10.3390/s22155646.

[6] A. Min, N. Nguyen, L. Howatt, M. Tavares, and J. Seo, "Aeroponic systems design: considerations and challenges," Journal of Agricultural Engineering, vol. 54, no. 1, 2023, doi: 10.4081/jae.2022.1387.

[7] A. D. Salsabila, A. E. U. Salam, F. A. Samman, D. Utamidewi, I. R. Sahali, and M. Itasari, "Control and monitoring system for aeroponic lettuce spraying using logistic regression," in Proc. 2024 FORTEI-International Conference on Electrical Engineering (FORTEI-ICEE), 2024, pp. 301–305, doi: 10.1109/FORTEI-ICEE64706.2024.10824456.

[8] H. Siebald, O. Hensel, H.-H. Kaufmann, and S. M. Kirchner, "Spray nozzle function control using acoustics for agricultural applications," Biosystems Engineering, vol. 197, pp. 149–155, 2020, doi: 10.1016/j.biosystemseng.2020.07.002.

[9] V. dos Santos Carreira, D. Nuyttens, J. Langenakens, J. V. Pereira, and R. P. da Silva, "Smartphone image-based framework for quick, non-invasive measurement of spray characteristics," Smart Agricultural Technology, vol. 3, Art. no. 100120, 2023, doi: 10.1016/j.atech.2022.100120.

[10] P. Acharya, T. Burgers, and K.-D. Nguyen, "A deep-learning framework for spray pattern segmentation and estimation in agricultural spraying systems," Scientific Reports, vol. 13, Art. no. 7545, 2023, doi: 10.1038/s41598-023-34320-7.

[11] L. Jiao, D. Dong, H. Feng, X. Zhao, and L. Chen, "Monitoring spray drift in aerial spray application based on infrared thermal imaging technology," Computers and Electronics in Agriculture, vol. 121, pp. 135–140, 2016, doi: 10.1016/j.compag.2015.12.006.

[12] M. Çomaklı and B. Sayıncı, "A novel image-based method for measuring spray pattern distribution in a mechanical patternator," Agriculture, vol. 15, no. 22, Art. no. 2337, 2025, doi: 10.3390/agriculture15222337.

[13] S.-M. Oh, J. Park, J. Yang, Y.-G. Oh, and K.-W. Yi, "Smart classification method to detect irregular nozzle spray patterns inside carbon black reactor using ensemble transfer learning," Journal of Intelligent Manufacturing, vol. 34, no. 6, pp. 2729–2745, 2023, doi: 10.1007/s10845-022-01951-y.

[14] M. Medina, M. Fatouraie, and M. S. Wooldridge, "High-speed imaging studies of gasoline fuel sprays at fuel injection pressures from 300 to 1500 bar," SAE Technical Paper 2018-01-0294, 2018, doi: 10.4271/2018-01-0294.

[15] F. Rosignoli and L. Postrioti, "Experimental validation of an innovative approach for GDI spray pattern recognition," Fuels, vol. 2, no. 1, pp. 16–36, 2021, doi: 10.3390/fuels2010002.

[16] L. Mopuri, V. Grahn, D. Sedarsky, and J. Hyvönen, "Shape/penetration analysis and comparisons of isolated spray plumes in a multi-hole Diesel spray," Experiments in Fluids, vol. 65, Art. no. 92, 2024, doi: 10.1007/s00348-024-03829-6.

[17] K. P. Sudheer and R. K. Panda, "Digital image processing for determining drop sizes from irrigation spray nozzles," Agricultural Water Management, vol. 45, no. 2, pp. 159–167, 2000, doi: 10.1016/S0378-3774(99)00079-7.

[18] S. Vulgarakis Minov, F. Cointault, J. Vangeyte, J. G. Pieters, and D. Nuyttens, "Spray droplet characterization from a single nozzle by high speed image analysis using an in-focus droplet criterion," Sensors, vol. 16, no. 2, Art. no. 218, 2016, doi: 10.3390/s16020218.

[19] S. Cryer and J. Raymond, "Interpreting image patterns for agricultural sprays using statistics and machine learning techniques," Fluids, vol. 9, no. 2, Art. no. 40, 2024, doi: 10.3390/fluids9020040.

[20] Raspberry Pi Ltd., "Raspberry Pi 4 Model B specifications," [Online]. Available: https://www.raspberrypi.com/products/raspberry-pi-4-model-b/specifications/. Accessed: May 22, 2026.